



Synthesis and antimicrobial evaluation of a pyrazoline-pyridine silver(I) complex: DNA-interaction and anti-biofilm activity

Dimitris Matiadis · Maria Karagiaouri · Barbara Mavroidi · Katarzyna E. Nowak · Georgios Katsipis · Maria Pelecanou · Anastasia Pantazaki · Marina Sagnou

Received: 22 June 2020 / Accepted: 19 October 2020 / Published online: 6 November 2020
© Springer Nature B.V. 2020

Abstract The emergence of resistant bacterial strains mainly due to misuse of antibiotics has seriously affected our ability to treat bacterial illness, and the development of new classes of potent antimicrobial agents is desperately needed. In this study, we report the efficient synthesis of a new pyrazoline-pyridine containing ligand **L1** which acts as an NN-donor for the formation of a novel silver (I) complex **2**. The free ligand did not show antibacterial activity. High potency was exhibited by the complex against three Gram-negative bacteria, namely *Escherichia coli*, *Pseudomonas aeruginosa* and *Acinetobacter baumannii* with the minimum inhibitory concentration

(MIC) ranging between 4 and 16 µg/mL (4.2–16.7 µM), and excellent activity against the fungi *Candida albicans* and *Cryptococcus neoformans* (MIC ≤ 0.25 µg/mL = 0.26 µM). Moreover, no hemolytic activity within the tested concentration range was observed. In addition to the planktonic growth inhibition, the biofilm formation of both Methicillin-resistant *Staphylococcus aureus* (MRSA) and *Pseudomonas aeruginosa* was significantly reduced by the complex at MIC concentrations in a dose-dependent manner for *Pseudomonas aeruginosa*, whereas a biphasic response was obtained for MRSA showing that the sub-MIC doses enhanced biofilm formation before its reduction at higher concentration. Finally, complex **2** exhibited strong DNA binding with a large drop in DNA viscosity indicating the absence of classical intercalation and suggesting the participation of the silver ion in DNA binding which may be related to its antibacterial activity. Taken together, the current results reveal that the pyrazoline-pyridine silver complexes are of high interest as novel antibacterial agents, justifying further in vitro and in vivo investigation.

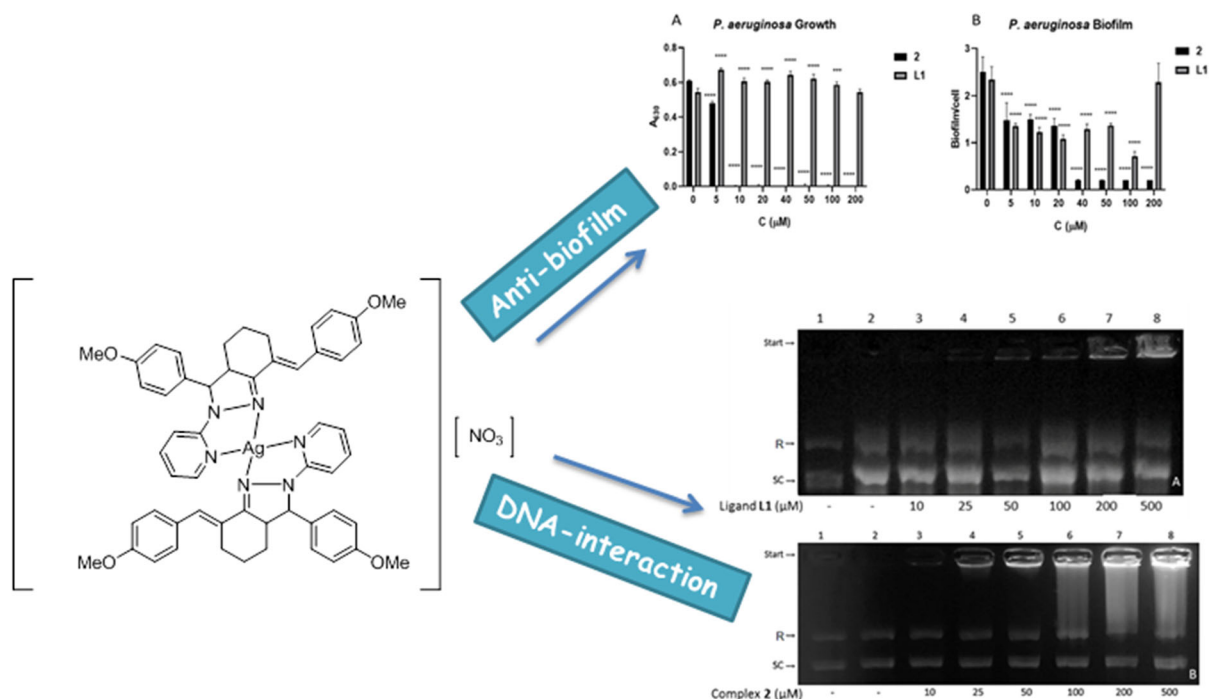
Electronic supplementary material The online version of this article (<https://doi.org/10.1007/s10534-020-00263-z>) contains supplementary material, which is available to authorized users.

D. Matiadis · B. Mavroidi · M. Pelecanou · M. Sagnou (✉)
National Centre for Scientific Research “Demokritos”,
Institute of Biosciences and Applications, Athens, Greece
e-mail: sagnou@bio.demokritos.gr

M. Karagiaouri · G. Katsipis · A. Pantazaki
Department of Chemistry, Laboratory of Biochemistry,
Aristotle University of Thessaloniki, 54124 Thessaloniki,
Greece

K. E. Nowak
Department of Molecular Biophysics, Faculty of Biology
and Environmental Protection, University of Lodz,
Pomorska St. 141/143, 90-236 Lodz, Poland

Graphic abstract



Keywords Silver complexes · NN donors · Pyrazoline-pyridine · Antimicrobial · DNA binding · Anti-biofilm

Introduction

Nowadays the preparation of novel antibacterial agents has become a priority because of the presence of multidrug-resistant pathogens (WHO factsheet 2018). The biological activity of metal complexes has, therefore, attracted increasing research interest over the years. Among them, the antibacterial, anti-fungal, and antiviral properties of silver ions, silver compounds, and, recently, silver nanoparticles have been extensively studied (Liang et al. 2018). The use of silver ions (Ag^+) in medical ointments, coating materials or even as additive in drinking water for antimicrobial and disinfectant purposes is known from the ancient ages (Barillo and Marx 2014). Silver salt solutions, mostly AgNO_3 have been used for bacterial infections associated with burn wounds or eye infections (Maillard et al. 2013). However, even though silver ions are considered potent and safe, they are

quickly reduced to metallic silver Ag^0 in the skin from the action of reducing agents, like thiols (Dabrowiak 2017). An effective way to control this extensive reduction is to react silver ions with a metal chelating moiety of an organic ligand resulting in a silver complex of desired physical, chemical, and/or biological properties able to “release” the silver ions to the medium.

Over the years, various such compounds have been presented (Fig. 1) with the commercially available as topical antibiotic cream, silver sulfadiazine (AgSD) being the most important. Sold under brand names, such as Silvadene, Silvazine and Sylfio, it is very effective against *Pseudomonas aeruginosa* and methicillin-resistant *Staphylococcus aureus* (MRSA) to prevent and treat wound infections (Fox and Modak 1974). At the research level, some silver complexes have exhibited better inhibitory activity than the first line treatments, such as a coumarin bearing Ag –N-heterocyclic carbene (NHC) with MIC in the range of 2–4 $\mu\text{g}/\text{mL}$ against *S. aureus*, *Escherichia coli* and *P. aeruginosa* (Achar et al. 2018) and a silver carboxylate complex incorporating anthracene moiety which demonstrated better activities against *Candida albicans*, *E. coli* and MRSA than ketoconazole and AgSD

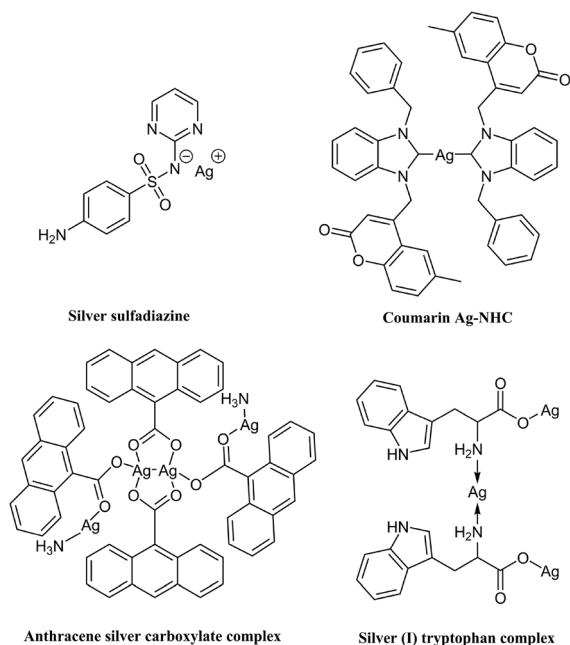


Fig. 1 Representative examples of antimicrobial silver (I) complexes

respectively (Curran et al. 2007). Moreover, Kazachenko and Legler (2000) reported that a silver (I)-N-ligand complex with tryptophan inhibits effectively a broad spectrum of pathogens with lowest MIC for *E. coli* (0.1 $\mu\text{g}/\text{mL}$) and low toxicity. Furthermore, recent work on silver(I) derivatives of several thio-ligands showed significant antimicrobial activity and low cellular toxicity with a high percent of cell viability (Aulakh, et al. 2018, 2020). Additionally, Favarin et al (2019) recently described the synthesis of novel mononuclear silver(I) complexes based on thiocarbamoyl-pyrazoline ligands which were proved selective for Gram-positive bacteria, after being tested against two standard bacterial strains: *S. aureus* ATCC 25,923 and *E. coli* ATCC 25,922. The MICs of free ligands were in the range of 125–375 $\mu\text{g}/\text{mL}$, whereas the values from 1.95 to 15.6 $\mu\text{g}/\text{mL}$ obtained for silver complexes are indicative of good activity, evidencing that metalation potentiated the antimicrobial activity.

Even though the mechanism of antimicrobial activity of silver(I) complexes has not been clearly elucidated (Kyros et al. 2014) an increasing amount of evidence suggests that silver has a broad range of biological targets and this is connected with a low probability of development of microorganism resistance against silver (Silver 2003). The low cell toxicity

and the reduced resistance are highly advantageous features prompting for the development of more efficient and convenient silver agents, in which employing ligands that can strongly coordinate to the active silver(I) ion.

The ability of pathogens to form sessile communities able to adhere to biotic or abiotic surfaces, known as biofilms, contributes to the microbial survival under hostile environments (Li and Lee 2017). In biofilms, microbial cells are embedded in a self-synthesized matrix consisting of extracellular polymeric substance (EPS) which is formed by polysaccharides, proteins, lipids, and extracellular DNA (e-DNA) as well as molecules originating from the host, such as mucus and DNA (Yang et al. 2012). Bacterial cells inside the biofilm are thousand times more resistant to the conventional antibiotics than the free-living forms and they are also tolerant against the immune response (Højby et al. 2010). The work of Nikodinovic-Runic and coworkers revealed the activity of silver (I) phthalazine, quinazoline and 1,5-naphthyridine to effectively inhibit *P. aeruginosa* and *C. albicans* biofilm formation (Glišić et al. 2016; Đurić et al. 2019).

Inspired by the aforementioned scientific evidence, we developed a novel pyridinyl pyrazoline as a strong NN bidentate chelator for the silver ion. The coordination of pyridine-bearing pyrazoles and pyrazolines to different metal centers has been shown to be a successful approach to increase biological activity of the ligand resulting in more potent compounds (Budzisz et al. 2009; Kupcewicz et al. 2013; Havrylyuk et al. 2020; Wang et al. 2011). The aim of our study was to prepare the first silver(I) complex of this class of compounds and investigate the structural and stability characteristics by means of NMR, DFT calculations, UV/Vis and thermogravimetry (TGA). The novel silver complex was further evaluated for its potential antibacterial and antifungal activity as well as its biofilm inhibition. Moreover, the DNA in vitro interactions, the hemolytic potential, and cytotoxic activity against non-cancerous cells have been also assessed.

Materials and methods

General

All reagents were purchased from Sigma-Aldrich and TCI and used without further purification. Melting

points were determined with a Gallenkamp MFB-595 melting point apparatus. NMR spectra were recorded with a Bruker Avance 500 MHz spectrometer operating at 500 MHz (^1H) and 125 MHz (^{13}C). Chemical shifts are reported in ppm relative to DMSO- d_6 (^1H : $\delta = 2.50$ ppm, ^{13}C : $\delta = 39.52 \pm 0.06$ ppm) and atom numbering for the ligand **L1** is available in the ESI. UV–Vis spectra were recorded with a Hitachi U-3010 spectrophotometer. IR spectra were recorded on a Perkin-Elmer Spectrum 100-IR spectrophotometer. HRMS spectra were recorded on UHPLC LC-MSn Orbitrap Velos-Thermo instrument in the Institute of Biology, Medicinal Chemistry and Biotechnology of the National Hellenic Research Foundation. Perkin Elmer, Pyris 1, system was used to run the simultaneous Thermogravimetric Analysis (TGA) experiments. The instrument mass precision is 1 μg . High purity air was used at a constant flow rate of 30 $\text{mL}\cdot\text{min}^{-1}$, depending on the conditions required for the experiments. A PerkinElmer 2400 CHNS Organic Elemental Analyzer 100 V was employed for the elemental analysis.

For single-point preliminary inhibitory assays, solutions of the samples were prepared in DMSO and water to a final testing concentration of 32 $\mu\text{g}/\text{mL}$, in 384-well, non-binding surface plate (NBS) for each bacterial/fungal strain, and in duplicate ($n = 2$), and keeping the final DMSO concentration to a maximum of 1% DMSO. All the sample preparation was done using liquid handling robots. Colistin and vancomycin were used as positive bacterial inhibitor standards for Gram-negative and Gram-positive bacteria, respectively. Fluconazole was used as a positive fungal inhibitor standard for *C. albicans* and *C. neoformans*.

The compound **2**, which was “flagged” as active in the preliminary screening was then serially diluted 1:twofold for 8 times. Each sample concentration was prepared in 384-well plates, non-binding surface plate (NBS; Corning 3640) for each bacterial/fungal strain, tissue-culture treated (TC-treated; Corning 3712/3764) black for mammalian cell types and polypropylene 384-well (PP; Corning 3657) for haemolysis assays, all in duplicate ($n = 2$), and keeping the final DMSO concentration to a maximum of 0.5%.

Thermal melting and viscosity experiments were carried out using calf thymus DNA (CT-DNA, Sigma Aldrich, USA) in phosphate buffer (0.05 M, pH = 7.2) consisting of $\text{Na}_2\text{HPO}_4\cdot 7\text{H}_2\text{O}$ and K_2HPO_4 . The

DNA concentration per nucleotide was determined spectrophotometrically by using the molar absorption coefficient of $e = 6600 \text{ M}^{-1} \text{ cm}^{-1}$ per nucleotide at 260 nm. Stock solutions of either CT-DNA or **L1** and complex **2** (in DMSO at a concentration of 10^{-2} M) were prepared prior each measurement and the corresponding mixtures were incubated for 24 h at 25 $^\circ\text{C}$ to reach the equilibrium state. Each reported measurement value is the average of three independent experiments.

Agarose was purchased from Invitrogen. Tryptone and yeast extract were purchased from Oxoid (Unipath Ltd., Hampshire, UK). Native DNA (dsDNA) (CT-DNA) type I, highly polymerized from calf thymus gland (D-1501) and the intercalative dye ethidium bromide (EthBr) (E1510) were purchased from Sigma.

Chemical synthesis

Intermediate derivative 2,6-bis((E)-4-methoxybenzylidene)cyclohexan-1-one (**1**), was synthesized following a published procedure (Matiadis et al. 2020).

(E)-7-(4-methoxybenzylidene)-3-(4-methoxyphenyl)-2-pyridyl-3,3a,4,5,6,7-hexahydro-2H-indazole (*L1*)

To a refluxing mixture of **1** (167 mg, 0.50 mmol) in absolute ethanol (9 mL) was dropwise added a solution of 2-hydrazinopyridine (273 mg, 2.50 mmol) in absolute ethanol (1 mL). After stirring under reflux for 72 h, the mixture was left to cool at room temperature. The precipitate solid was filtered under vacuum, washed carefully with cold ethanol and dried to afford the desired product as light yellow solid. Yield 125 mg (59%), UV–Vis (DMSO) λ_{max} (log ϵ): 337 (4.31), FTIR (KBr, cm^{-1}): 2930, 1590, 1510, 1475, 1440, 1246, 1185, 1030, 835, 770, 355, ^1H NMR (500 MHz, DMSO- d_6): 1.43 (1H, m, H-14), 1.67 (1H, m, H-15), 1.86 (1H, m, H-14), 2.08 (1H, m, H-15), 2.44 (1H, m, H-13), 2.86 (1H, m, H-13), 2.91 (1H, m, H-4), 3.72 (3H, s, OCH_3 (H-32)), 3.78 (3H, s, OCH_3 (H-24)), 4.91 (1H, d, $J = 11.2$ Hz, H-5), 6.72 (1H, t, $J = 6.0$ Hz, H-9), 6.88 (2H, d, $J = 8.5$ Hz, H-27/H-29), 6.97 (2H, d, $J = 8.5$ Hz, H-19/H-21), 7.10 (1H, s, H-16), 7.23 (2H, d, $J = 8.5$ Hz, H-26/H-30), 7.38 (2H, 2 \times d overlapped, $J = 8.5$ Hz, H-7 and H-18/H-22), 7.58 (1H, t, $J = 7.4$ Hz, H-8), 7.92 (1H, d, $J = 4.2$ Hz, H-10), ^{13}C NMR (125 MHz, DMSO- d_6): 23.7 (C-14), 28.4 (C-13), 28.9 (C-15), 55.0 (MeO(C-32)), 55.1

(MeO(C-24)), 56.2 (C-4), 69.6 (C-5), 110.7 (C-7), 113.8 (C-27/C-29), 113.9 (C-19/C-21), 115.2 (C-9), 125.5 (C-16), 126.8 (C-26/C-30), 128.6 (C-17), 128.9 (C-12), 130.9 (C-18/C-22), 135.5 (C-25), 136.9 (C-8), 147.0 (C-10), 155.3 (C-3), 157.1 (C-6), 158.0 (C-28), 158.5 (C-20); HRMS: calcd for $[C_{27}H_{28}N_3O_2 + H]^+$ 426.2182; found 426.2170.

$[Ag(L1)_2][NO_3] (2)$

To a stirring solution of pyrazoline **L1** in dry DCM (8 mL) was added dropwise a solution of $AgNO_3$ (51 mg, 0.30 mmol) in CH_3CN (2 mL). The reaction mixture was stirred in the dark under nitrogen at r.t. 16 h. n-Hexane (10 mL) was added in the mixture and left for 1 h at r.t. The dark brown precipitate that formed was filtered and the filtrate was evaporated under vacuum at under 35 °C. The formed film was washed with diethyl ether (4 mL) and then dissolved in the minimum amount of methanol. Diethyl ether was added until a small amount of dark brown precipitate was formed. Finally, the mixture was filtered and the filtrate was evaporated to yield a bright yellow solid. Yield 74 mg (51%), UV–Vis (DMSO) λ_{max} (log ϵ), 344 (4.73), FTIR (KBr, cm^{-1}): 2930, 2345, 2120, 1750–1870, 1600, 1510, 1480, 1431, 1300, 1241, 1173, 1017, 833, 765, 545, 1H NMR (500 MHz, DMSO- d_6): 1.40 (2H, m, H-15/H-14), 1.85 (1H, m, H-14), 1.96 (1H, m, H-15), 2.38 (1H, m, H-13), 2.87 (1H, m, H-13), 2.98 (1H, m, H-4), 3.75 (3H, s, OMe(H-32)), 3.81 (3H, s, OMe(H-20)), 4.31 (1H, br, H-5), 6.35 (1H, d, $J = 8.5$ Hz, H-7), 6.90–6.97 (7H, H-9/H-18/H-19/H-21/H-22/H-27/H-29), 7.18 (2H, d $J = 8.2$ Hz, H-26/H-30), 7.24 (1H, s, H-16), 7.63 (1H, t, $J = 7.4$ Hz, H-8), 8.38 (1H, d, $J = 4.2$ Hz, H-10), ^{13}C NMR (125 MHz, DMSO- d_6): 23.1 (C-14), 27.9 (C-15), 28.5 (C-13), 55.1 (OMe(C-32)), 55.3 (OMe(C-20)), 56.3 (C-4), 70.1 (C-5), 109.1 (C-7), 114.0, 114.7 (C-19/C-21, C-27/C-29), 116.2 (C-9), 126.9 (C-26/C-30), 127.3 (C-16), 127.8 (C-17), 131.1 (C-18/C-22), 132.3 (C-25), 139.1 (C-8), 149.2 (C-10), 154.5 (C-6), 156.1 (C-3), 158.9 (C-28), 159.0 (C-20), Elemental Analysis found (calcd): C, 63.46 (63.53); H, 5.40 (5.33); Ag, 10.57 (10.46); N, 9.64 (9.71); O, 10.93 (10.97); HRMS: calcd for $[C_{54}H_{54}^{109}AgN_6O_3]$ 959.3254; found 959.3548.

Computational methods

The geometries of cationic part of complex **2** (and ligand **L1** for comparison) were pre-optimized using the Molecular Mechanics (MM) method. Then, in the DFT calculations the Becke3-Lee-Parr (B3LYP) functional (Becke 1993; Lee et al. 1988) with LANL2DZ (Dunning Jr et al. 1977; Hay and Wadt 1985a, b; Wadt and Hay. 1985) basis set were used. The hybrid B3LYP functional along with this basis set was applied to study of silver (I)-organic ligand complexes reported in the literature (Fomuta et al. 2017; Altürk et al. 2017). All calculations were performed using Gaussian 03 program package (Frisch et al. 2004).

Biological evaluation

Antimicrobial assay

All bacteria were cultured in Cation-adjusted Mueller Hinton broth (CAMHB) at 37 °C overnight. A sample of each culture was then diluted 40-fold in fresh broth and incubated at 37 °C for 1.5–3 h. The resultant mid-log phase cultures were diluted (Colony Forming Units—CFU/mL measured by OD_{600}), then added to each well of the compound containing plates, giving a cell density of 5×10^5 CFU/mL and a total volume of 50 μ L. All the plates were covered and incubated at 37 °C for 18 h without shaking.

Inhibition of bacterial growth was determined measuring absorbance at 600 nm (OD_{600}), using a Tecan M1000 Pro monochromator plate reader. The percentage of growth inhibition was calculated for each well, using the negative control (media only) and positive control (bacteria without inhibitors) on the same plate as references. The significance of the inhibition values was determined by modified Z-scores, calculated using the median and Median Absolute Deviation (MAD) of the samples (no controls) on the same plate.

For single-point preliminary screening, samples with inhibition > 80% and Z-Score above 2.5 for either replicate ($n = 2$ on different plates) when tested at 32 μ g/mL were classed as actives. Samples with inhibition values between 50 and 80% and Z-Score above 2.5 for either replicate ($n = 2$ on different plates) were classed as partial actives.

The minimum inhibitory concentration (MIC) of **2** was determined as the lowest concentration at which the growth was fully inhibited in the dose response assay (0.25–32 µg/mL), defined by an inhibition $\geq 80\%$. 80% value is used to allow for the fluctuation of growth that is typically 10–20% for any given bacterial or fungi assay.

Antifungal assay

Fungi strains were cultured for 3 days on Yeast Extract-Peptone Dextrose (YPD) agar at 30 °C. A yeast suspension of 1×10^6 to 5×10^6 CFU/mL (as determined by OD₅₃₀) was prepared from five colonies. The suspension was subsequently diluted and added to each well of the compound-containing plates giving a final cell density of fungi suspension of 2.5×10^3 CFU/mL and a total volume of 50 µL. All plates were covered and incubated at 35 °C for 24 h without shaking.

Growth inhibition of *C. albicans* was determined measuring absorbance at 530 nm (OD₅₃₀), while the growth inhibition of *C. neoformans* was determined measuring the difference in absorbance between 600 and 570 nm (OD₆₀₀₋₅₇₀), after the addition of resazurin (0.001% final concentration) and incubation at 35 °C for additional 2 h. The absorbance was measured using a Biotek Synergy HTX plate reader. The percentage of growth inhibition was calculated for each well, using the negative control (media only) and positive control (fungi without inhibitors) on the same plate. The significance of the inhibition values was determined by modified Z-scores, calculated using the median and MAD of the samples (no controls) on the same plate.

For single-point preliminary screening, samples with inhibition $> 80\%$ and Z-Score above 2.5 for either replicate ($n = 2$ on different plates) when tested at 32 µg/mL were classed as actives. Samples with inhibition values between 50 and 80% and Z-Score above 2.5 for either replicate ($n = 2$ on different plates) were classed as partial actives.

The MIC of the active compound **2** was determined as the lowest concentration at which the growth was fully inhibited in the dose–response assay (0.25–32 µg/mL), defined by an inhibition $\geq 80\%$ for *C. albicans* and an inhibition $\geq 70\%$ for *C. neoformans*. Due to a higher variance in growth and

inhibition, a lower threshold was applied to the data for *C. neoformans*.

Cytotoxicity assay

Cytotoxicity to human embryonic kidney cells (HEK293) was determined using the resazurin assay as previously described (O'Brien et al. 2000; McMillan et al. 2002). Briefly, HEK293 cells were counted manually in a Neubauer hemocytometer and then plated in the 384-well plates containing the compound **2** at an 8-point dose–response (0.25–32 µg/mL) to give a density of 5000 cells/well in a final volume of 50 µL Dulbecco's Modified Eagle Medium (DMEM) supplemented with 10% Fetal Bovine Serum (FBS) was used as growth media and the cells were incubated together with the compounds for 20 h at 37 °C in 5% CO₂.

Cytotoxicity (or cell viability) was measured by fluorescence, ex: 560/10 nm, em: 590/10 nm (F_{560/590}), after addition of 5 µL of 25 µg/mL resazurin (2.3 µg/mL final concentration) and after incubation for further 3 h at 37 °C in 5% CO₂. The fluorescence intensity was measured using a Tecan M1000 Pro monochromator plate reader, using an automatic gain calculation.

CC₅₀ (concentration at 50% cytotoxicity) was calculated by curve fitting the inhibition values vs log(concentration) using a sigmoidal dose–response function, with variable fitting values for the bottom, top, and slope. In addition, the maximal percentage of cytotoxicity is reported as D_{Max}, indicating any compounds with partial cytotoxicity.

The curve fitting was implemented using Pipeline Pilot's dose–response component, resulting in similar values to curve fitting tools such as GraphPad's Prism and IDBS's XIFit. Any value with $>$ indicate samples with no activity (low D_{Max} value) or samples with CC₅₀ values above the maximum tested concentration (higher D_{Max} value).

Cytotoxic samples were classified by CC₅₀ ≤ 32 µg/mL in either replicate ($n = 2$ on different plates).

Hemolysis assay

Human whole blood was washed three times with 3 volumes of 0.9% NaCl and then re-suspended in the same solution to a concentration of 0.5×10^8 cells/

mL, as determined by manual cell count in a Neubauer hemocytometer and used for hemolysis assay as previously described (Ravipati et al. 2015). Briefly, the washed cells were then added to the 384-well compound-containing plates at an 8-point dose–response (0.25–32 µg/mL) for a final volume of 50 µL. After a 10 min agitation on a plate shaker the plates were then incubated for 1 h at 37 °C. After incubation, the plates were centrifuged at 1000 g for 10 min to pellet cells and debris, 25 µL of the supernatant was then transferred to a polystyrene 384-well assay plate.

Hemolysis was determined by measuring the supernatant absorbance at 405 nm (OD_{405}). The absorbance was measured using a Tecan M1000 Pro monochromator plate reader.

HC_{10} and HC_{50} (concentration at 10% and 50% hemolysis, respectively) were calculated by a curve fitting the inhibition values vs log(concentration) using a sigmoidal dose–response function with variable fitting values for top, bottom, and slope. In addition, the maximal percentage of hemolysis is reported as D_{Max} , indicating any compounds with partial hemolysis.

The curve fitting was implemented using Pipeline Pilot's dose–response component, resulting in similar values to curve fitting tools such as GraphPad's Prism and IDBS's XIFit. Any value with > indicate samples with no activity (low D_{Max} value) or samples with HC_{10} values above the maximum tested concentration (higher D_{Max} value).

Hemolysis samples were classified by $HC_{10} \leq 32$ µg/mL in either replicate ($n = 2$ on different plates). In addition, samples were flagged as partial hemolytic if $D_{Max} \geq 50\%$, even with $HC_{10} >$ the maximum tested concentration.

Inhibition of biofilm formation

The ability of MRSA and *P. aeruginosa* ATCC 27,853 to form biofilm in the presence of newly synthesized compounds were tested. Bacteria were grown overnight at 37 °C, in an LB growth medium. Cultures were then diluted 100-times with Tryptone Soybean Broth (TSB) for biofilm formation of MRSA, or with 4-times diluted TSB (TSB/4) for biofilm formation of *P. aeruginosa*. Concentrations of either complex **2** or **L1** (5, 10, 20, 40, 50, 100 or 200 µM) in 200 µl of each sample were transferred in an SPL 96-well

microplate. The plate was left still at 37 °C for 24 h. The growth of the cells was measured using an Elisa reader at 630 nm. The cells not attached to the plate were washed away three times with 10 mM phosphate-buffered saline solution, pH 7.4 (PBS) and left to dry for 1 h at 50–60 °C. Crystal violet (CV) (200 µL) solution (0.1%, v/v) were then added in each well and the plate was left at room temperature for 15 min. The dye was washed away thoroughly with tap water, and the plate was left to dry for one more hour at 50–60 °C. Acetic acid 33% (v/v) (200 µL) was finally added to extract bound dye and the absorbance was measured at 570 nm, using an Elisa reader (BioTek Instruments Inc., USA). All samples tested contain the same DMSO concentration and a sample containing DMSO only was also run as a control.

DNA binding studies

Thermal denaturation: DNA melting experiments were carried out by monitoring the absorbance of DNA at 258 nm in the temperature range from 25.0 °C to 95.0 °C and temperature was increased at a 0.5 °C/min rate. The melting temperature (T_m) of DNA was determined as the midpoint of the optically detected transition and the measurement was repeated three times for each sample. The thermal melting experiments were performed in phosphate buffer solution (final percentage of DMSO = 2%) by keeping the DNA concentration constant (5×10^{-5} M) while varying the concentration of **L1** and complex **2** (0 – 2.5×10^{-5} M) to achieve ratios $R = [\text{compound}] / [\text{DNA}]$ of 0, 0.01, 0.05, 0.1, 0.33, 0.5.

Viscosity studies

Viscosity measurements were carried out using Ostwald's viscometer (Schott geräte, type 531 01/0a, thermostat Schott geräte GT 1150, meter Schott geräte AVS 300) at 25 °C. The viscometer was thermostated at 25.0 ± 0.1 °C in a constant temperature bath. Flow time of solutions was measured with a digital stopwatch and each sample was measured three times and an average flow time was calculated. The values did not differ by more than 0.2 s from each other. All solutions were filtered through a 0.22 µm filter (Millipore, Billerica, MA) prior to the measurements. Experiments were carried out in phosphate buffer solution (final percentage of DMSO = 2%) by keeping

the DNA concentration constant (5×10^{-5} M) while varying the concentration of **L1** and complex **2** (0 – 2.5×10^{-5} M) to achieve ratios $R = [\text{compound}]/[\text{DNA}]$ of 0, 0.02, 0.033, 0.05, 0.1, 0.2, 0.5. The intrinsic viscosity $[\eta]$ was calculated according to the relation $[\eta] = (t - t_b)/t_b$, where t_b is the flow time for the buffer and t is the observed flow time for DNA in the presence or absence of the compounds. Data were presented as $(\eta/\eta_0)^{1/3}$ versus R where η and η_0 are the intrinsic viscosities in the presence or absence of the compounds. For the low DNA concentrations used in these experiments, the intrinsic viscosity $[\eta]$ is proportional to the difference in the flow times for the buffer with and without DNA, resulting in the following Eq. (1) (Cohen, and Eisenber 1969):

$$\frac{L}{L_0} = \frac{[\eta]^{1/3}}{[\eta_0]^{1/3}} = \frac{(t - t_b)^{1/3}}{(t_0 - t_b)^{1/3}} \quad (1)$$

where L and L_0 are the DNA lengths and $[\eta]$ and $[\eta_0]$ are the intrinsic viscosities with and without the compound. The t_b , t_0 and t are the flow times of the buffer, the plain DNA and the DNA/compound solution, respectively.

DNA binding by agarose gel electrophoresis

The compound efficiency for interaction with pDNA was measured by determining its ability initially, to convert the supercoiled DNA (SC) or the relaxed form (R) of the pDNA to the nicked circular (NC) or/and linear form, and furthermore with CT-DNA to cause up-shift or complete degradation. Reactions, which contained aliquots of 10 μg of each nucleic acid (plasmid pCR2.1 or CT-DNA), were incubated at a constant temperature of 37 $^\circ\text{C}$ in the presence of various concentrations of the compound in a buffer A to a final volume of 20 μL . The reaction was terminated by the addition of 5 μL loading buffer consisting of 0.25% w/v bromophenol blue and 30% v/v glycerol in water. The products resulting from interactions of the compound with DNA were separated by electrophoresis on agarose gel (1% w/v), which contained 0.5 $\mu\text{g}/\text{mL}$ EtBr in 40 mM Tris–acetate, pH 7.5, 20 mM sodium acetate, 2 mM Na_2EDTA . Electrophoresis was carried out for 90 min at 5 V cm^{-1} , in a horizontal gel apparatus (Mini-SubTM DNA Cell, BioRad). The gels were visualized and photographed under a UV illuminator,

based on the excitation of EtBr-DNA complex. All samples tested contain the same DMSO concentration and a sample containing DMSO only was also run as control.

Results and discussion

Synthesis

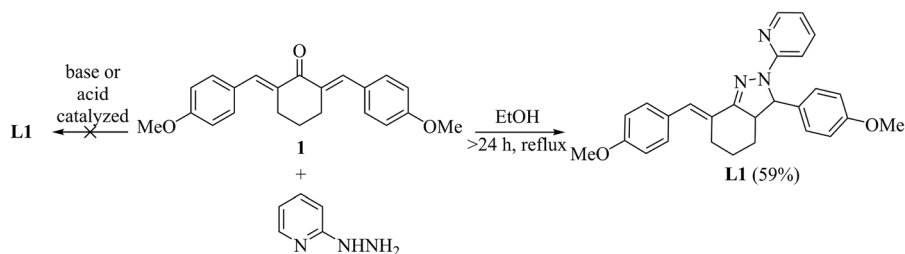
1-Pyridine-2-pyrazoline **L1** was synthesized via the cyclization reaction between 2-hydrazinopyridine and the appropriate symmetrical monocarbonyl curcuminoid, 2,6-bis[(*E*)-4-methoxybenzylidene]-cyclohexan-1-one **1**, which was obtained from cyclohexanone and *p*-anisaldehyde following a previously published method [10].

The optimal conditions for the cyclization reaction proved to be ethanol as a solvent and reflux for 72 h, while the product **L1** can be obtained in satisfactory yields ($\sim 35\%$) after 24 h of reflux (Scheme 1). The use of glacial acetic acid or bases, both weak (CH_3COONa) and strong (EtONa) proved to be ineffective resulting, respectively, in very low yields ($< 25\%$), no formation of product, or traces of inseparable products. The pyrazoline **L1** was prepared in pure form and used without further purification.

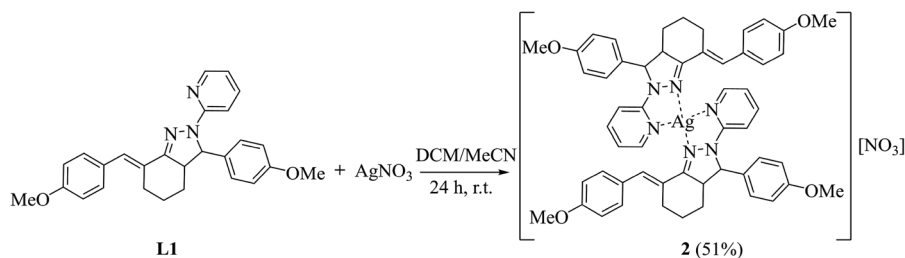
The reaction of pyridyl-pyrazoline **L1** with silver nitrate in dichloromethane:acetonitrile in ratio $\text{AgNO}_3:\text{L1} = 1:2$ at room temperature for 24 h yielded the complex $[\text{Ag}(\text{L1})_2]\text{NO}_3$ **2** (Scheme 2). The silver compound **2** was obtained as a bright yellow amorphous solid, which can be stored at r.t. without taking any special precaution regarding the light or humidity (see below).

Both the ligand **L1** and the silver complex **2** were fully characterized by ^1H , ^{13}C and 2D NMR spectroscopy. The assignments are listed in the experimental section. While most of the ^{13}C peaks display only minor shifts (-3.2 to $+2.2$ ppm), some ^1H peaks appear significantly shielded or deshielded after complexation. The characteristic α -hydrogen of the pyridine unit (H-10, see Supporting information for numbering) shifted to low field ($+0.46$ ppm) suggesting the coordination of the silver (I) ion through the N-donor atom of the pyridine.

Infrared spectra of the pyrazoline-pyridine moiety of **L1** showed intense band for $\nu(\text{C}=\text{N})$ at 1590 cm^{-1} , which was shifted to 1600 cm^{-1} in



Scheme 1 Synthesis of compound **L1**



Scheme 2 Synthesis of silver (I) complex **2**

complex **2**, suggesting the participation of nitrogen atoms of pyridine and 2-pyrazoline rings in coordination with the metal ions. Moreover, the appearance of strong absorptions in the regions 1476–1431, and 1246–1186 cm^{-1} as well as the shift from 1030 cm^{-1} to 1017 cm^{-1} may be assigned to $\text{C}=\text{N}$ - and $\text{C}-\text{N}$ -moieties of pyrazoline and pyridine rings and the result of metal complexation. Also an additional band at 545 cm^{-1} appears in IR spectra, which is the characteristic band of $\text{M}-\text{N}$ stretching.

In the UV/Vis absorption spectrum of **L1** in DMSO a strong peak at $\lambda_{\text{max}} = 337 \text{ nm}$ and $\varepsilon = 2.04 \times 10^4 \text{ M}^{-1} \text{ cm}^{-1}$ was observed whereas complex **2** in DMSO (Figure S5) showed a maximum absorption peak at $\lambda_{\text{max}} = 344 \text{ nm}$ with $\varepsilon = 5.37 \times 10^4 \text{ M}^{-1} \text{ cm}^{-1}$. These peaks can be assigned to $\pi-\pi^*$ transitions of the highly conjugated arylidene pyrazolo-pyridine system. The increase in both λ_{max} and ε upon complexation provide clear evidence of ($\text{C}=\text{N}$) coordination to the metal ion.

The metal to ligand ratio was determined by HRMS analysis, which also revealed the isotopic abundance of 109-Ag in the complex, whereas, taking into account the neutral charge of the ligand, the presence of the nitrate counterion was determined by elemental analysis. Unfortunately, even after numerous attempts, no single crystals suitable for X-ray crystallographic analysis were obtained.

Thermogravimetric and Differential Thermal Gravimetric (TG/DTG) analysis of the active compound **2** was carried out from room temperature to 700 $^{\circ}\text{C}$ under air with a heating rate of 10 $^{\circ}\text{C}/\text{min}$. The TGA measurements showed that compound **2** was stable up to 175 $^{\circ}\text{C}$ (Fig. 2). After that temperature, the decomposition was observed in three stages (Table 1). The first stage took place at 175–205 $^{\circ}\text{C}$ revealing a weight loss of 6.73%. The second weight loss of 20.71% occurred at 220–383 $^{\circ}\text{C}$. The last step from 383 to 522 $^{\circ}\text{C}$ corresponds to the complete decomposition of the ligand and the formation of the silver oxide as the final residue. The total weight loss of 86.15% is close to the calculated value of 88.65%.

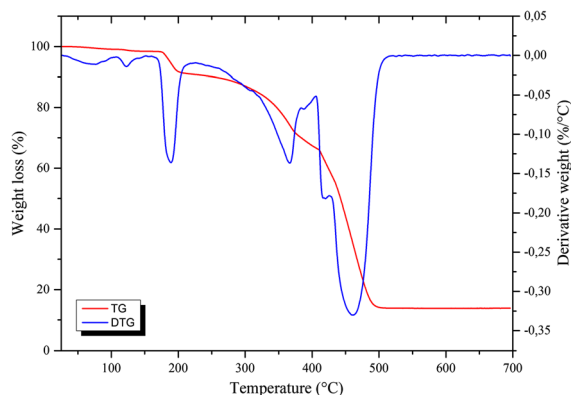


Fig. 2 TG/DTG thermodiagram of Ag (I) complex **2**

Table 1 Thermal analysis data including temperature range, DT peak, weight loss and proposed segment

Compound	Temp range (°C)	Peak temp (°C)	Weight loss (%)
complex 2	175–205	189	6.73
	220–383	366	20.71
	383–522	460	86.15 ^[a]

^[a]The %value represents the total weight loss for the decomposition of the ligand and oxidation of the silver ion to silver oxide

Computations

Molecular structures of the cationic part of complex **2** (and ligand **L1**) obtained in the gas phase using DFT/B3LYP/LANL2DZ method are shown in Fig. 3. Selected structural parameters of the cation of complex molecule are presented in Table S4 (Supporting Information). There is no experimental structural data either for the complex or ligand, so it is not possible to compare theoretical and experimental results for the investigated systems. As can be seen in Fig. 3, both ligand and cationic part of complex structures are non-planar, as expected. In the complex molecule the two ligands are coordinated to the central silver(I) ion via bonds with nitrogen atoms (Fig. 3). The lengths of Ag–N bond range from 2.294 to 2.454 Å and the bite angles N–Ag–N are equal $\sim 71^\circ$. These B3LYP/LANL2DZ calculated values of distances and angles around the Ag atom are in good agreement with experimental values reported for similar silver(I) complexes (Ovejero et al. 2013; Cifuentes-Vaca et al. 2019).

Electronic properties of ligand **L1** and the cation of complex **2** calculated at the B3LYP/LANL2DZ level of theory, are presented in Table 2. It can be seen that the ligand molecule is more polar than the complex molecule, the HOMO and LUMO energies obtained for the cation of complex have significantly lower

values compared to those for the ligand, and their energy gap is lower for $[\text{Ag}(\text{L1})_2]^+$ compared to that of **L1**.

Stability

The stability of complex **2** in solid state and in solution was determined by UV/Vis and ^1H NMR studies. The UV/Vis spectra in DMSO showed no significant changes occurring over 24 h (Figure S5) suggesting complex stability in this solvent. When the same experiments were repeated in aqueous 1% DMSO solution, a small but not negligible decrease in the absorption over all the wavelength range, without any change in the pattern of the original spectrum, was observed (Figure S6). Additionally, solid samples stored at r.t. under standard storage conditions, protected from light, air and humidity, over a period of six months, displayed unaltered ^1H NMR and UV/Vis spectra.

However, prolonged dissolution in organic solvents such as DCM, CHCl_3 , Et_2O and others, regardless of light conditions, resulted in the precipitation of a dark amorphous solid suggesting the dissociation of the coordination compound.

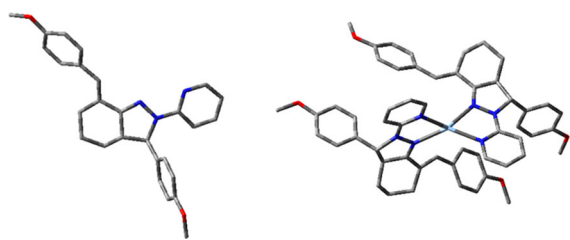


Fig. 3 B3LYP/LANL2DZ optimized structures of ligand **L1** and cation of complex **2** (hydrogen atoms have been omitted for clarity)

Table 2 B3LYP/LANL2DZ calculated properties of the ligand **L1** and cation of complex **2**

Property	L1	$[\text{Ag}(\text{L1})_2]^+$
$\mu[\text{D}]$	6.7	4.1
E_{HOMO} [eV]	– 4.959	– 7.304
E_{LUMO} [eV]	– 1.339	– 3.980
E_{g} [eV]	3.62	3.32

Antimicrobial evaluation

The starting compound **1**, the ligand **L1** and the complex **2**, were screened against 5 key ESKAPE pathogens, the Gram-negative *E. coli*, *K. pneumoniae*, *A. baumannii*, *P. aeruginosa*, and the Gram-positive methicillin-resistant *S. aureus* as well as the fungi *C. albicans* and *C. neoformans*. At single point concentration of 32 µg/mL, both **1** and **L1** showed no activity in any strain, whereas the silver complex **2** proved active against both bacteria and fungi. Next, an 8-point dose response (0.25–32 µg/mL) antimicrobial activity assay was performed for complex **2** in duplicate to confirm the activity and to determine the minimum inhibitory concentration (MIC). The MIC was determined following the CLSI guidelines, identifying the lowest concentration at which full inhibition of the bacteria or fungi was observed. Full inhibition of growth has been defined at ≤ 20% growth (or > 80% inhibition). Complex **2** displayed moderate to high activity on Gram-negative bacteria *E. coli* (MIC = 8 µg/mL = 8.3 µM), *P. aeruginosa* (MIC = 16 µg/mL = 16.6 µM) and *A. baumannii* (MIC = 4 µg/mL = 4.15 µM) and very high potency against *C. albicans* and *C. neoformans* (both MIC ≤ 0.25 µg/mL) (Table 3). Finally, the MIC value achieved against the Gram-positive methicillin-resistant *S. aureus* was > 32 µg/mL. Among the tested pathogens, higher activity was observed against the Gram-negative species compared to the Gram-positive, a result that is not entirely unusual, as higher activity for Gram-negative has been reported before (Nawaz et al. 2011; Njogu, et al. 2017). This is, however, the exact

opposite to the results reported by Favarin et al. (2019) which indicates the significance of the ligand nature in the specific antimicrobial activity of the silver complexes. Moreover, it exhibits outstanding antifungal activity. It is worth noting, that mixed ligand silver(I) complexes of triphenylphosphine and heterocyclic thiones (imidazolidine-2-thione (Imt), diazinane-2-thione (Diaz) and 2-mercaptopyridine (Mpy)), silver(I) complexes of phosphate and hydroxymethylene derivatives of pyridine and (benz)imidazole, silver(I)-thienylterpyridine and silver(I)-furylterpyridine complexes and some N-(pyridinylmethylene)aniline silver (I) complexes were found to be less active than our complex (Nawaz et al. 2011; Kalinowska-Lis et al. 2016; Njogu et al. 2017, 2018). Consequently, the 2-pyridyl-pyrazoline moiety acts as an efficient NN donor to coordinate silver in such a way to allow silver ion to exert antimicrobial and antifungal activity.

An additional highly desirable and advantageous feature of complex **2** was that no hemolysis was observed with HC₅₀ > 32 µg/mL. Despite this low hemolytic activity which is an indication of low toxicity, a value of CC₅₀ = 7.31 µM for the mammalian HEK-293 cytotoxicity was measured which is marginally lower or equal to the MIC values obtained. However, as silver ion-containing agents usually find applications in wound dressings and topical antimicrobial or antifungal creams that exhibit low systemic toxicity due to poor absorption through the skin (Enna and Bylund 2008), the observed toxicity in the HEK-293 line may well not contradict the further biological application of complex **2** which will be explored

Table 3 Antimicrobial activity as Minimum Inhibitory Concentration (MIC), cytotoxicity (CC₅₀) and hemolytic activity (HC₅₀) of the starting compound **1**, the ligand **L1** and the silver (I) complex **2**^[a]

Compound	Sa	Ec	Kp	Pa	Ab	Ca	Cn	CC ₅₀	HC ₅₀
1	> 32	> 32	> 32	> 32	> 32	> 32	> 32	nd ^[b]	nd
L1	> 32	> 32	> 32	> 32	> 32	> 32	> 32	nd	nd
2	> 32	8	> 32	16	4	≤ 0.25	≤ 0.25	7.31	> 32
Chloramphenicol	8	8	> 32	> 32	> 32	> 32	> 32	-	> 32
Fluconazole	> 32	> 32	> 32	> 32	> 32	0.125	8	-	> 32
AgNO ₃	≤ 0.25	≤ 0.25	≤ 0.25	≤ 0.25	≤ 0.25	≤ 0.25	≤ 0.25	-	> 32

^[a]Sa: Methicillin-resistant *Staphylococcus aureus*, Ec *Escherichia coli*, Kp *Klebsiella pneumoniae*, Pa *Pseudomonas aeruginosa*, Ab *Acinetobacter baumannii*, Ca *Candida albicans*, Cn *Cryptococcus neoformans*

^[b]not determined

through in vivo tests. Moreover, it is worth mentioning that most of the antifungal agents have been found to be fairly toxic against mammalian cells, like amphotericin B (Hamil 2013).

Inhibition of biofilm formation

The effect of increasing concentrations of complex **2** and **L1**, on the ability of bacterial cells, either MRSA or *P. aeruginosa*, to form a biofilm, as well as on the growth of the bacterial population of planktonic cells, was also evaluated, and the results are presented in Figs. 4 and 5, respectively. In the case of MRSA growth, **L1** did not alter the bacterial planktonic cells population even at the highest concentration tested.

On the other hand, complex **2** inhibited MRSA growth at concentrations higher than 20 μM in a dose-dependent manner. This is in agreement with our former results since MIC was higher than 32 $\mu\text{g}/\text{mL}$ (33.4 μM). Regarding the biofilm formation effect of the two compounds some interesting results were observed. The ligand **L1** resulted in an initial increase in biofilm formation, which was almost doubled at 20 μM and remained at this high level for the rest of the concentrations tested. It is noteworthy, that in the presence of **L1** the free-floating cells coexist with an increasing biofilm community, suggesting that even though the ligand does not effectively reduce the planktonic MRSA population, it still creates a highly hostile microenvironment forcing the bacteria towards

the biofilm formation as a defense adaptation. In the case of complex **2**, a biphasic response to increasing concentrations was recorded for biofilm formation. At low concentrations, below 20 μM , the biofilm formation remained low and unaltered, whereas a dramatic increase, reaching almost a threefold rise, occurred at 20 μM , followed by a gradual biofilm inhibition at higher doses reaching almost complete biofilm elimination at 200 μM . As it was observed for **L1** the free-floating cells and biofilm population coexist. However, it is interesting to note that below 20 μM there is only a small and steady biofilm mass which is almost half the population occurring in the presence of **L1** despite the fact that the planktonic population is almost the same in both conditions. Assuming that both **L1** and complex **2** have comparable ability to create a hostile microenvironment, an analogous increase in biofilm population could be expected. However, this is not the case, indicating either that complex **2** does not stress the free-floating cells enough to force them towards the biofilm formation or that it exhibits a direct antibiofilm potential establishing some kind of dynamic equilibrium between the planktonic and biofilm forms. The dramatic increase in biofilm formation at the sub-inhibitory concentration of the 20 μM , which seems to be very critical, is in agreement with the mounting evidence suggesting that *S. aureus* responds to sub-inhibitory concentrations of antibiotic by inducing biofilm formation and changing its biofilm matrix composition (Schilcher et al. 2016;

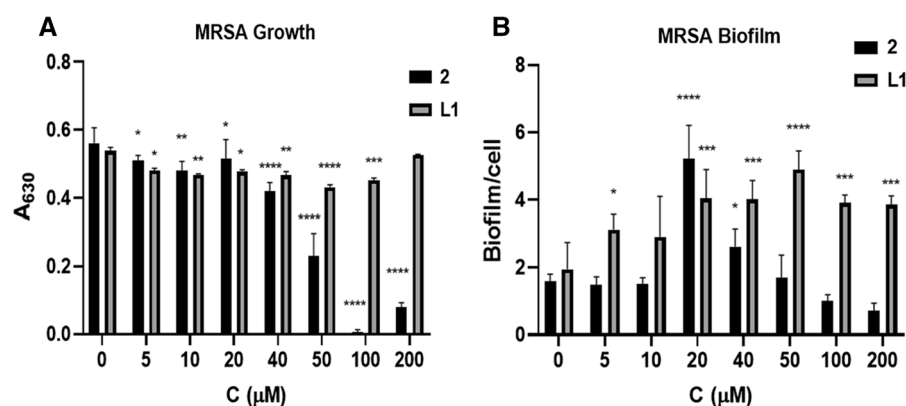


Fig. 4 Growth of planktonic MRSA and biofilm production in the presence of different concentrations of complex **2** or **L1**. Overnight grown bacteria (200 μL) diluted with TSB, were added in each well and the plate was further incubated for 24 h at 37 $^{\circ}\text{C}$. The growth was measured by the absorbance at 630 nm (A). After that, the plate was washed and stained with

0.1% (w/v) CV, and the biofilm production was measured at 570 nm; (B). The absorbance was measured using an Elisa reader. Two-way ANOVA analysis (Graph Pad Prism 8) for differences between treated and non-treated bacteria: * $p < 0.05$, ** $p < 0.01$, *** $p < 0.001$, **** $p < 0.0001$

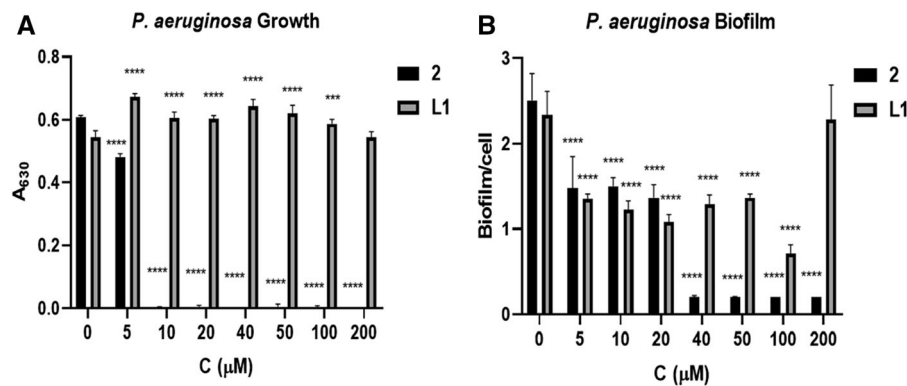


Fig. 5 *P. aeruginosa* cells growth and biofilm production in the presence of different concentrations of complex **2** or **L1**. Overnight grown bacteria (200 µL) diluted with TSB, were added in each well and the plate was further incubated for 24 h at 37 °C. The growth absorbance was measured at 630 nm (A). After that the plate was washed and stained with 0.1% (w/v) CV

and the biofilm production was measured at 570 nm; (B). The absorbance was measured using an Elisa reader. Two-way ANOVA analysis (Graph Pad Prism 8) for differences between treated and non-treated bacteria: * $p < 0.05$, ** $p < 0.01$, *** $p < 0.001$, **** $p < 0.0001$

Shang et al. 2019). As expected at concentrations $> \text{MIC}$ the decrease in the growth of the planktonic cells appears to follow a similar trend to the biofilm inhibition, suggesting that the latter is closely related to the reduced free-floating population in addition to the anti-biofilm activity.

With respect to the effect of **L1** on *P. aeruginosa* planktonic cells growth and biofilm production, Fig. 5 clearly shows that the planktonic population remained unaffected. In contrast to the MRSA response, however, in complex **2**, at concentrations $\geq 10 \mu\text{M}$, the *P. aeruginosa* free-floating bacterial population was eradicated. Moreover, treatment with complex **2** resulted in a dose-dependent decrease in biofilm formation. This observation suggests the increased potency of complex **2** against the planktonic population and the establishment of a hostile environment at concentrations 5–20 µM leading to some steady biofilm formation. Interestingly, at a concentration range between 40 and 200 µM there is still a small but persistent population of cells in the biofilm form, when no planktonic cells are observed. At higher concentrations, the bacteria were not able to survive or create any biofilm. In the case of **L1**, the initial biofilm population was nearly halved at 5–50 µM concentration, and it finally recovered to its initial level.

The work by Bjarnsholt et al. (2007) has given us results on the activity of silver and its complexes, including silver sulfadiazine, against *P. aeruginosa* biofilms suggesting that the bactericidal concentration

of silver needed to eliminate the bacterial biofilm was between 10 and 100 times greater than that used to eliminate planktonic bacteria. Our results are in good agreement with these findings as there is a tenfold increase in the concentration needed to eliminate completely the biofilm population compared to the 10 µM required to eradicate the planktonic bacteria. Interestingly, Sullivan et al. reached an opposite conclusion in their study of phenanthroline-silver complexes a fact that could be related to the nature of the phenanthroline moiety (Sullivan et al. 2014).

DNA binding studies

DNA is the target of large number of pharmacologically active drug molecules, and the biological activity of several antibacterial drugs is directly related to DNA binding and inhibition of DNA replication (Waring 1991; Shahabadi and Hashempour, 2019). Therefore, the DNA interaction of ligand **L1** and complex **2** was assessed through thermal denaturation and viscosity measurements.

Thermal denaturation studies can provide information about the mode and the strength of the interaction between DNA and compounds present in solution. With increasing temperature, the double-stranded DNA gradually dissociates to single strands and hyperchromicity is observed in its UV spectra, attributed to increased absorption of the unstacked bases. Both the melting temperature T_m (the

temperature at which 50% of the double helix denatures into single-stranded DNA) and the hyperchromicity h increase are affected by the interaction of DNA with compounds in solution. For CT-DNA alone, under our experimental conditions, a T_m of 70.03 ± 0.11 °C and an % increase of hyperchromicity (% h) of 30.1 ± 0.5 °C were recorded, values that are in good agreement with the literature values (Chandramouli et al. 2004). The effect of different concentrations of **L1** and its Ag complex **2** on the melting temperature of CT-DNA is presented in Table 4, along with the associated % h . In the presence of increasing concentrations of **L1**, both the T_m values and the % h were not significantly altered, indicating lack of any major interaction with the CT-DNA structure. However, addition of the silver complex **2** resulted in reduction of the T_m values compared to the CT-DNA control, in addition to a decrease of % h , reaching a ΔT_m value of -2.8 °C and % h value of 24.9%, at the highest ratio of $R = 0.5$, indicative of interaction of DNA with complex **2**. The lower T_m observed excludes interaction through classical intercalation that is accompanied by a substantial increase in T_m ranging from $+4$ °C to $+14$ °C (Pramanik et al. 2016) and suggests alternative modes of DNA binding.

To further clarify the nature of the binding interaction, the hydrodynamic method of viscosimetry which is sensitive to the length of DNA was employed. Groove binding typically results in only subtle changes in structure, and DNA remains essentially in its native form. In contrast, classical intercalation with insertion of a planar ligand moiety between adjacent base pairs, results in lengthening of DNA with concomitant increase in viscosity (Suh & Chaires 1995). As shown in Fig. 6, upon addition of **L1** no significant changes in the relative viscosity of DNA

were observed indicating lack of interaction. However, co-incubation of increasing amounts of complex **2** with CT-DNA resulted in a gradual and significant decrease of viscosity reaching a value of 0.7 at the ratio of [compound]/DNA = 0.5. This significant drop in viscosity indicates a significant decrease in the axial length of DNA which may be ascribed to Ag^+ —DNA interaction. Previous studies have demonstrated that Ag^+ ions interact strongly with nitrogen atoms in DNA bases, affecting the local DNA structure and significantly reducing the apparent DNA length (Bain et al. 2017; Jiang and Ran 2018). The presence of a positive charge on complex **2** may facilitate its approach to the DNA helix through ionic interaction with the negatively charged phosphate backbone, thus enabling the interaction of Ag^+ ions with the bases in the grooves. Various modes of interaction of silver complexes with DNA have been reported in the literature, apparently shaped by the specific physical and chemical properties of each complex. Mixed ligand silver(I) complexes have been reported to interact strongly with either the minor or major groove of CT-DNA through theoretical docking studies (Banti et al. 2012, 2015; Sainis et al. 2016). On the contrary, silver(I)–thienylterpyridine and silver(I)–furylterpyridine complexes significantly increased the viscosity of DNA solutions implying an intercalating mode of binding (Njogu et al. 2018). Similarly, silver (I) complexes of benzimidazole open-chain ether ligands and some V-shaped bis-benzimidazole ligands and their silver (I) complexes were shown to bind to DNA in an intercalative mode, supported by the presence of large planar aromatic rings, hydrogen bonds, and π - π stacking interactions (Wu et al. 2012, 2015). Finally, the silver pyridine-2-sulfonate complexes were reported to interact with DNA by a dual binding mode: partial intercalation along with

Table 4 Thermal denaturation data (ΔT_m and % h) for CT-DNA in the presence of **L1** and complex **2** (\pm SD in parenthesis)

	R = 0		R = 0.01		R = 0.05		R = 0.1		R = 0.33		R = 0.5	
	ΔT_m (°C)	% h										
L1	0	30.1 (0.5)	0.24 (0.01)	28.4 (2.3)	0.23 (0.01)	29.1 (1.9)	0.28 (0.02)	29.7 (2.9)	0.25 (0.01)	28.7 (2.1)	0.29 (0.02)	28.9 (3.2)
2	0	30.1 (0.5)	-0.20 (0.02)	28.9 (3.6)	-0.83 (0.08)	27.1 (3.8)	-1.50 (0.09)	25.9 (1.6)	-1.99 (0.10)	25.1 (2.9)	-2.89 (0.26)	24.9 (3.2)

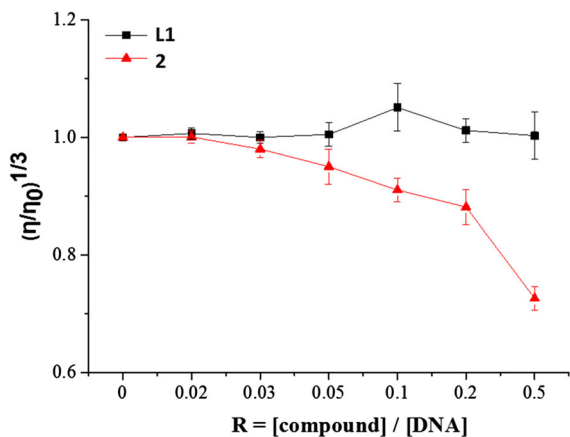


Fig. 6 Effects of increasing amounts of **L1** and complex **2** on the relative viscosity of CT-DNA (5×10^{-5} M) at 25 °C with ratios $R = \text{compound} / [\text{DNA}]$ ranging from 0 to 0.5

groove binding (Rendošová et al. 2018). To the best of our knowledge, this is the first time that experimental data support the interaction of the silver ion core of a complex with DNA bases.

The DNA-binding activity was also assessed by gel electrophoresis of CT-DNA. Knowing that the charge, flexibility, and size of DNA play an important role in its movement on the agarose gel, DNA binding of a compound causes it to move more slowly on the gel, because the bound DNA is transformed into a larger structure of higher molecular weight than the free DNA, and the total charge of DNA is reduced (Anjomshoa et al. 2015). Electrophoresis of CT-DNA after its incubation with the silver complex **2** (Fig. 7B) confirms its ability to bind to the CT-DNA double helix as it was previously shown by the physicochemical methods. This can be witnessed by both the slight decrease in the mobility of the DNA bands which creates a visible upshift of the zone in each lane, at the presence of increasing amounts of complex **2** (lanes 3–8) and the intensification of the UV signal, compared to the untreated DNA without (lane 1) or with the same amount of DMSO (lane 2). Both the decrease of the DNA band mobility and the intensification occur in a concentration-dependent manner. On the other hand, ligand **L1** does not appear to interact with CT-DNA, as indicated by comparison of the zone of lane 2 (DNA treated only with DMSO) with the following lanes.

The interaction of complex **2** (Fig. 6b) or **L1** (Fig. 6a) with DNA was also tested with the plasmid

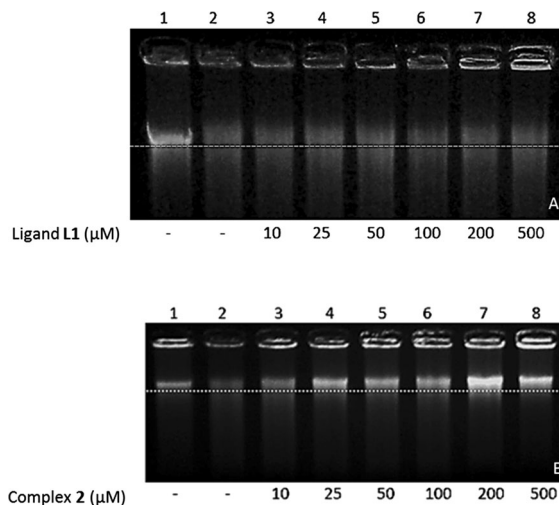


Fig. 7 DNA mobility shift. 10 µg of CT-DNA was treated with the same volume of DMSO (lane 2) and increasing concentration of **L1** (A) or complex **2** (B). The samples were incubated for 30 min at 37 °C and then analyzed on a 1% w/v agarose gel electrophoresis

DNA pCR2.1. Compound **2** interacts with both forms of pDNA, which is shown by the concentration-dependent upshift (lanes 3–8) in comparison to the untreated DNA (lane 1) or DNA treated only with DMSO (lane 2). However, the interaction with the supercoiled form (SC) of the plasmid is much weaker compared to that with the relaxed form. This is clearly obvious at the higher concentrations tested (100, 200 and 500 µM) (lanes 6–8) where the relaxed pDNA band (R) appears diffused and upshifted, while a smaller degree of upshift is noted at the SC form, in comparison with interaction with DMSO only (lane 2). This difference may be attributed to the tightly-packed structure of the supercoiled molecule which probably does not allow many binding sites to be accessible on its outer surface compared to those of the relaxed form. Similar decreased mobility of the pBR322 plasmid DNA gel bands with increasing Ag + concentration, indicating the occurrence of increased binding of silver ions with DNA was observed by Hossain and Huq (Hossain and Huq 2002). Incubation with **L1** does not affect to any significant degree neither pDNA mobility nor UV intensity.

In conclusion, this is the first time that a newly synthesized pyridine-pyrazoline has been shown to act as a highly promising NN chelating moiety to accommodate the silver ion. The resulting complex exhibits moderate to high antimicrobial activity

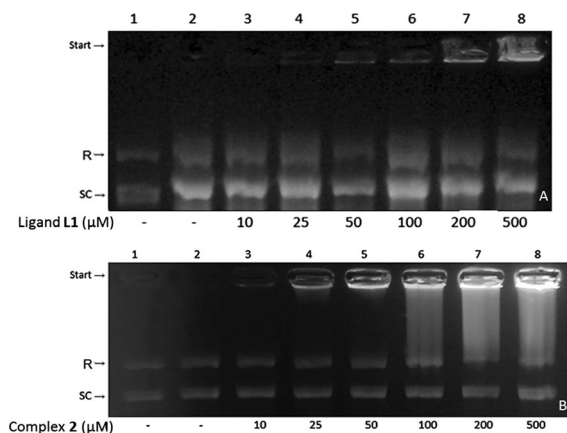


Fig. 8 pDNA mobility. 10 μ g pCR2.1 DNA was treated with the same volume of DMSO (lane 2) and increasing concentration of **L1** (A) or complex **2** (B). The samples were incubated for 30 min at 37 $^{\circ}$ C and then analyzed on a 1% w/v agarose gel electrophoresis

against Gram-negative bacteria, moderate antimicrobial activity against Gram-positive bacteria and excellent anti-fungal properties. The cytotoxicity profile of the complex is moderate with no hemolysis being observed which prompts us for further investigation. Complex **2** additionally shows an excellent ability to eradicate bacterial biofilm at MIC concentrations. Based on our results, the complex exhibits strong DNA binding potential, with evidence provided by viscosimetry on the participation of silver anion in interaction with the DNA bases. Further investigation on the mode of action of complex **2** is on the way to provide insights into possible structural optimizations towards increased antibacterial/antifungal potency.

Acknowledgements Antimicrobial and mammalian cell toxicity screening was performed by CO-ADD (The Community for Open Antimicrobial Drug Discovery) (Blaskovich 2015), funded by the Wellcome Trust (UK) and The University of Queensland (Australia). The calculations were performed on a computer in the Laboratory of Computer and Analytical Techniques, University of Lodz (Poland). DM and BM were supported by a scholarship co-financed by Greece and the European Union (European Social Fund- ESF) through the Operational Programme «Human Resources Development, Education and Lifelong Learning» in the context of the project “Reinforcement of Postdoctoral Researchers—2nd Cycle” (MIS-5033021), implemented by the State Scholarships Foundation (IKY).

References

- Achar G, Shahini CR, Patil SA, Malecki JG, Pan SH, Lan A, Chen XR, Budagumpi S (2018) Sterically modulated silver (I) complexes of coumarin substituted benzimidazol-2-ylidenes: Synthesis, crystal structures and evaluation of their antimicrobial and antitumor cancer potentials. *J Inorg Biochem* 183:43–57. <https://doi.org/10.1016/j.jinorgbio.2018.02.012>
- Altürk S, Avci D, Tamer Ö, Atalay Y (2017) DFT calculations on spectroscopic, structural and NLO properties of silver (I) complex with picolinamide. *AIP Conf Proc* 1815:100001. <https://doi.org/10.1063/1.4976464>
- Anjomshoa M, Hadadzadeh H, Fatemi SJ, Torzadeh-Mahani M (2015) A mononuclear Ni(II) complex with 5,6-diphenyl-3-(2-pyridyl)-1,2,4-triazine: dNA- and BSA-binding and anticancer activity against human breast carcinoma cells. *Spectrochim Acta A Mol Biomol Spectrosc* 136:205–215. <https://doi.org/10.1016/j.saa.2014.09.016>
- Aulakh JK, Lobana TS, Sood H, Arora DS, Garcia-Santos I, Kaur M, Jasinski JP (2020) Synthesis, structures, and novel antimicrobial activity of silver (I) halide complexes of imidazolidine-2-thiones. *Polyhedron* 175:114235. <https://doi.org/10.1016/j.poly.2019.114235>
- Aulakh JK, Lobana TS, Sood H, Arora DS, Smolinski VA, Duff CE, Jasinski JP (2018) Synthesis, structures, and ESI-mass studies of silver(I) derivatives of imidazolidine-2-thiones: Antimicrobial potential and biosafety evaluation. *J Inorg Biochem* 178:18–31. <https://doi.org/10.1016/j.jinorgbio.2017.10.002>
- Bain D, Paramanik B, Patra A (2017) Silver(I) induced conformation change of DNA: gold nanocluster as spectroscopic probe. *J Phys Chem C* 121:4608–4617. <https://doi.org/10.1021/acs.jpcc.6b10560>
- Banti CN, Hadjikakou SK (2013) Anti-proliferative and antitumor activity of silver(I) compounds. *Metallomics* 5:569–596. <https://doi.org/10.1039/c3mt00046j>
- Banti CN, Giannoulis AD, Kourkoumelis N, Owczarzak AM, Poyraz M, Kubicki M, Charalabopoulos K, Hadjikakou SK (2012) Mixed ligand-silver(I) complexes with anti-inflammatory agents which bind to lipoxygenase and calf-thymus DNA, modulating their function and inducing apoptosis. *Metallomics* 4:545–560. <https://doi.org/10.1039/C2MT20039B>
- Banti CN, Giannoulis AD, Kourkoumelis N, Owczarzak AM, Kubicki M, Hadjikakou SK (2015) Silver(I) Compounds of the anti-inflammatory agents salicylic acid and P-Hydroxyl-Benzoic acid which modulate cell function. *J Inorg Biochem* 142:132–144. <https://doi.org/10.1016/j.jinorgbio.2014.10.005>
- Barillo DJ, Marx DE (2014) Silver in medicine: a brief history BC 335 to present. *Burns* 40S:S3–S8. <https://doi.org/10.1016/j.burns.2014.09.009>
- Becke AD (1993) Density Functional Thermochemistry. III. The Role of Exact Exchange. *J Chem Phys* 98:5648–5652. <https://doi.org/10.1063/1.464913>
- Bjarnsholt T, Kirketerp-Møller K, Kristiansen S, Phipps R, Nielsen AK, Jensen PØ, Høiby N, Givskov N (2007) Silver against *Pseudomonas aeruginosa* biofilms. *APMIS*

- 115:921–928. https://doi.org/10.1111/j.1600-0463.2007.apm_646.x
- Budzisz E, Miernicka M, Lorenz I-P, Mayer P, Krajewska U, Rozalski M (2009) Synthesis and X-ray Structure of Platinum(II), Palladium(II) and Copper(II) Complexes with Pyridine-pyrazole Ligands: Influence of Ligands' Structure on Cytotoxic Activity. *Polyhedron* 28:637–645. <https://doi.org/10.1016/j.poly.2008.12.013>
- Chandramouli KH, Thimmaiah KN, Chandrashekar A, D'Souza CJM (2004) Interaction of 2-Chloro-N-Substituted Phenoxazine with DNA and Effect on DNA Melting. *Nucleosides Nucleotides Nucleic Acids* 23:1639–1656. <https://doi.org/10.1081/NCN-200031461>
- Cifuentes-Vaca OL, Andrades-Lagos J, Campanini-Salinas J, Laguna A, Vázquez-Velázquez D, Concepción Gimeno M (2019) Silver(I) and copper(I) complexes with a Schiff base derived from 2-aminofluorene with promising antibacterial activity. *Inorg Chim Acta* 489:275–279. <https://doi.org/10.1016/j.ica.2019.02.033>
- Cohen G, Eisenber H (1969) Viscosity and sedimentation study of sonicated DNA proflavine complexes. *Biopolymers* 8:45–55. <https://doi.org/10.1002/bip.1969.360080105>
- Curran R, Lenehan J, McCann M, Kavanagh K, Devereux M, Egan DA, Clifford G, Keane K, Creaven BS, McKee V (2007) $[Ag_2(aca)_2]n$ and $[Ag_4(aca)_4(NH_3)_2](acaH=9\text{-anthracenecarboxylic acid})$: Synthesis, X-ray crystal structures, antimicrobial and anti-cancer activities. *Inorg Chem Commun* 10:1149–1153. <https://doi.org/10.1016/j.inoche.2007.06.021>
- Dabrowiak JC (2017) *Metals in Medicine*, Chap 7. Wiley, Oxford UK
- Das S, Kumar GS (2008) Molecular aspects on the interaction of phenosafranine to deoxyribonucleic acid: Model for intercalative drug–DNA binding. *J Mol Struct* 872:56–63. <https://doi.org/10.1016/j.molstruc.2007.02.016>
- Dunning TH Jr, Hay PJ (1997) Gaussian Basis Sets for Molecular Calculations. In: Schaefer HF (ed) *Modern Theoretical Chemistry*, vol 3. Plenum, New York, pp 1–28
- Đurić S, Vojnović S, Pavić A, Mojicević M, Wadepohl H, Savić ND, Popsavin M, Nikodinović-Runic J, Djuran MI, Glišić BĐ (2020) New polynuclear 1,5-naphthyridine-silver(I) complexes as potential antimicrobial agents: The key role of the nature of donor coordinated to the metal center. *J Inorg Biochem* 203:110872. <https://doi.org/10.1016/j.jinorgbio.2019.110872>
- Enna SJ, Bylund DB (2008) *xPharm: The Comprehensive pharmacology reference*. Elsevier, Pittsburgh
- Favarin LRV, Oliveira LB, Silva H, Micheletti AC, Pizzuti L, Machulek-Júnior A, Caires ARL, Back DF, Lima SM, Andrade LHC, Duarte LFB, Pinto LMC, Casagrande GA (2019) Sonochemical Synthesis of Highly Luminescent Silver Complexes: Photophysical Properties and Preliminary in vitro Antitumor and Antibacterial Assays. *Inorg Chim. Acta* 492:235–242. <https://doi.org/10.1016/j.ica.2019.04.043>
- Fomuta TR, Ngoune J, Djimassar G, Djampou TA, Matemb JMNT, Anguile JJ, Nenwa J (2017) Synthesis, Rietveld Refinement and DFT Studies of Bis(4,5-di-hydro-1H-benzo[g]indazole)silver(I) Hexafluorophosphate Complex Salt. *Open J Inorg Chem* 7:102–115. <https://doi.org/10.4236/ojic.2017.74007>
- Fox CL, Modak SM (1974) Mechanism of Silver Sulfadiazine Action on Burn Wound Infections. *Antimicrob Agents Chemother* 5:582–588. <https://doi.org/10.1128/AAC.5.6.582>
- Frisch MJ, Trucks GW, Schlegel HB, Scuseria GE, Robb MA, Cheeseman JR, Montgomery J, Vreven T, Kudin KN, Burant JC, Millam NJ, Iyengar SS, Tomasi J, Barone V, Mennucci B, Cossi M, Scalmani G, Rega N, Petersson GA, Nakatsuji H, Hada M, Ehara M, Toyota K, Fukuda R, Hasegawa J, Ishida M, Nakajima T, Honda Y, Kitao O, Nakai H, Klene M, Li X, Knox JE, Hratchian HP, Cross JB, Bakken V, Adamo C, Jaramillo J, Gomperts R, Stratmann RE, Yazyev O, Austin AJ, Cammi R, Pomelli C, Ochterski JW, Ayala PY, Morokuma K, Voth GA, Salvador P, Dannenberg JJ, Zakrzewski VG, Dapprich S, Daniels AD, Strain MC, Farkas Ö, Malick DK, Rabuck AD, Raghavachari K, Foresman JB, Ortiz JV, Cui Q, Baboul AG, Clifford S, Cioslowski J, Stefanov BB, Liu G, Liashenko A, Piskorz P, Komaromi I, Martin RL, Fox DJ, Keith T, Al-Laham MA, Peng CY, Nanayakkara A, Challacombe M, Gill PMW, Johnson B, Chen W, Wong MW, Gonzalez C, Pople JA (2004) Gaussian 03, Revision D.01, Wallingford CT.
- Glišić BĐ, Senerović L, Comba P, Wadepohl H, Veselinović A, Miličević DR, Djuran MI, Nikodinović-Runic J (2016) Silver(I) complexes with phthalazine and quinazoline as effective agents against pathogenic *Pseudomonas aeruginosa* strains. *J Inorg Biochem* 155:115–128. <https://doi.org/10.1016/j.jinorgbio.2015.11.026>
- Hamil RJ (2013) Amphotericin B formulations: a comparative review of efficacy and toxicity. *Drugs* 73:919–934. <https://doi.org/10.1007/s40265-013-0069-4>
- Havrylyuk D, Heidary DK, Su, n Y, Parkin, S, Glazer E C, (2020) Photochemical and Photobiological Properties of Pyridyl-pyrazol(in)e-Based Ruthenium(II) Complexes with Sub-micromolar Cytotoxicity for Phototherapy. *ACS Omega* 5(30):18894–18906. <https://doi.org/10.1021/acsomega.0c02079>
- Hay PJ, Wadt WR (1985a) *Ab initio* effective core potentials for molecular calculations. Potentials for the transition-metal atoms Sc to Hg. *J Chem Phys* 82:270–283. <https://doi.org/10.1063/1.448799>
- Hay PJ, Wadt WR (1985b) *Ab initio* effective core potentials for molecular calculations. Potentials for K to Au including the outermost core orbitals. *J Chem Phys* 82:299–310. <https://doi.org/10.1063/1.448975>
- Højby N, Bjarnsholt T, Givskov M, Molin S (2010) Ciofu O Antibiotic resistance of bacterial biofilms. *Int J Antimicrob Agents* 35:322–332. <https://doi.org/10.1016/j.ijantimicag.2009.12.011>
- Hossain Z, Huq F (2002) Studies on the interaction between Ag(+) and DNA. *J Inorg Biochem* 91:398–404. [https://doi.org/10.1016/s0162-0134\(02\)00454-3](https://doi.org/10.1016/s0162-0134(02)00454-3)
- Jana B, Senapati S, Ghosh D, Bose D, Chattopadhyay N (2012) Spectroscopic Exploration of Mode of Binding of ctDNA with 3-Hydroxyflavone: A Contrast to the Mode of Binding with Flavonoids Having Additional Hydroxyl Groups. *J Phys Chem B* 116:639–645. <https://doi.org/10.1021/jp2094824>
- Jiang WY, Ran SY (2018) Two-stage DNA compaction induced by silver ions suggests a cooperative binding mechanism.

- J Chem Phys 148:205102. <https://doi.org/10.1063/1.5025348>
- Kalinowska-Lis U, Felczak A, Chęcińska L, Szablowska-Gadomska I, Patyna E, Małecki M, Lisowska K, Ochocki J (2016) Antibacterial Activity and Cytotoxicity of Silver(I) Complexes of Pyridine and (Benz) Imidazole Derivatives X-ray Crystal Structure of [Ag(2,6-di(CH₂OH)py)₂]NO₃. *Molecules* 21:87. <https://doi.org/10.3390/molecules21020087>
- Kazachenko AS, Legler AV, Per'yanova OV, Vstavskaya YA, (2000) Synthesis and antimicrobial activity of silver complexes with histidine and tryptophan. *Pharm Chem J* 34:257–258. <https://doi.org/10.1007/BF02524634>
- Kelly JM, Tossi AB, McConnell DJ, OhUigin C (1985) A study of the interactions of some polypyridylruthenium (II) complexes with DNA using fluorescence spectroscopy, topoisomerisation and thermal denaturation. *Nucl Acids Res* 13:6017–6034. <https://doi.org/10.1093/nar/13.17.6017>
- Kyros L, Banti CN, Kourkoumelis N, Kubicki M, Sainis I, Hadjikakou SK (2014) Synthesis, characterization, and binding properties towards CT-DNA and lipoxygenase of mixed-ligand silver(I) complexes with 2-mercaptothiazole and its derivatives and triphenylphosphine. *J Biol Inorg Chem* 19:449–464. <https://doi.org/10.1007/s00775-014-1089-6>
- Kupcewicz B, Ciolkowski M, Karwowski BT, Rozalski M, Krajewska U, Lorenz I-P, Mayer P, Budzisz E (2013) Copper(II) Complexes with Pyrazole Derivatives—Synthesis, Crystal Structure, DFT Calculations and Cytotoxic Activity. *J. Mol. Struct.* 1052:32–37. <https://doi.org/10.1016/j.molstruc.2013.08.055>
- Lee C, Yang W, Parr RG (1998) Development of the Colle-Salvetti correlation-energy formula into a functional of the electron density. *Phys Rev B* 37:785–789. <https://doi.org/10.1103/PhysRevB.37.785>
- Lerman LS (1961) Structural considerations in the interaction of DNA and acridines. *J Mol Biol* 3:18–30. [https://doi.org/10.1016/S0022-2836\(61\)80004-1](https://doi.org/10.1016/S0022-2836(61)80004-1)
- Li XH, Lee JH (2017) Antibiofilm agents: A new perspective for antimicrobial strategy. *J Microbiol* 55:753–766. <https://doi.org/10.1007/s12275-017-7274-x>
- Liang X, Luan S, Yin Z, He M, He C, Yin L, Zou Y, Yuan Z, Li L, Song X, Lv C, Zhang W (2018) Recent advances in the medical use of silver complex. *Eur J Med Chem* 157:62–80. <https://doi.org/10.1016/j.ejmech.2018.07.057>
- Maillard JY, Hartemann P (2013) Silver as an antimicrobial: facts and gaps in knowledge. *Crit Rev Microbiol* 39:373–383. <https://doi.org/10.3109/1040841X.2012.713323>
- Matiadis D, Mavroidi B, Panagiotopoulou A, Methenitis C, Pelecanou M, Sagnou M (2020) (E)-(1-(4-Ethoxycarbonylphenyl)-5-(3,4-dimethoxyphenyl)-3-(3,4-dimethoxyxytyryl)-2-pyrazoline: synthesis, characterization, DNA-interaction, and evaluation of activity against drug-resistant cell lines. *Molbank* 2020:M1114. <https://doi.org/10.3390/M1114>
- McMillan MK, Li L, Parker JB, Patel L, Zhong Z, Gunnett JW, Powers WJ, Johnson MD (2002) An Improved Resazurin-Based Cytotoxicity Assay for Hepatic Cells. *Cell Biol Toxicol* 18:157–173. <https://doi.org/10.1023/a:1015559603643>
- Nawaz S, Isab AA, Merz K, Vasylyeva V, Metzler-Nolte N, Saleem M, Ahmad S (2011) Synthesis, characterization and antimicrobial studies of mixed ligand silver(I) complexes of triphenylphosphine and heterocyclic thiones: Crystal structure of bis[$(\mu^2$ -diazinane-2-thione) (diazinane-2-thione)(triphenylphosphine)silver(I) nitrate]]. *Polyhedron* 30:1502–1506. <https://doi.org/10.1016/j.poly.2011.02.054>
- Njogu EM, Martincigh BS, Omondi B, Nyamori VO (2018) Synthesis, characterization, antimicrobial screening and DNA binding of novel silver(I)-thienylterpyridine and silver(I)-furylterpyridine complexes. *Appl Organometal Chem* 32:e4554. <https://doi.org/10.1002/aoc.4554>
- Njogu EM, Omondi B, Nyamori VO (2017) Silver(I)-pyridinyl Schiff base complexes: Synthesis, characterization and antimicrobial studies. *J Mol Struct* 1135:118–128. <https://doi.org/10.1016/j.molstruc.2017.01.061>
- O'Brien J, Wilson I, Orton T, Pognan F (2000) Investigation of the Alamar Blue (resazurin) fluorescent dye for the assessment of mammalian cell cytotoxicity. *Eur J Biochem* 267:5421–5426. <https://doi.org/10.1046/j.1432-1327.2000.01606.x>
- Ovejero P, Asensio E, Heras JV, Campo JA, Cano M, Torres MR, Núñez C, Lodeiro C (2013) Silver-pyrazole complexes as hybrid multifunctional materials with metal-omesogenic and photoluminescent behaviour. *Dalton Trans* 42:2107–2120. <https://doi.org/10.1039/C2DT31750H>
- Pramanik S, Chatterjee S, Saha A, Devi PS, Suresh Kumar G (2016) Unraveling the Interaction of Silver Nanoparticles with Mammalian and Bacterial DNA. *J Phys Chem B* 120:5313–5324. <https://doi.org/10.1021/acs.jpcc.6b01586>
- Ravipati AS, Henriques ST, Poth AG, Kaas Q, Wang CK, Colgrave ML, Craik DJ (2015) Lysine-rich cyclotides: a new subclass of circular knotted proteins from violaceae. *ACS Chem Biol* 10:2491–2500. <https://doi.org/10.1021/acschembio.5b00454>
- Rendošová M, Vargová Z, Sabolová D, Imrichová N, Hudecová D, Gyepes R, Lakatoš B, Elefantová K (2018) Silver pyridine-2-sulfonate complex - its characterization, DNA binding, topoisomerase I inhibition, antimicrobial and anticancer response. *J Inorg Biochem* 186:206–216. <https://doi.org/10.1016/j.jinorgbio.2018.06.006>
- Sainis I, Banti CN, Owczarzak AM, Kyros L, Kourkoumelis N, Kubicki M, Hadjikakou SK (2016) New antibacterial, non-genotoxic materials, derived from the functionalization of the anti-thyroid drug methimazole with silver ions. *J Inorg Biochem* 160:114–124. <https://doi.org/10.1016/j.jinorgbio.2015.12.013>
- Schilcher K, Andreoni F, Dengler Haunreiter V, Seidl K, Hasse B, Zinkernagel AS (2016) Modulation of *Staphylococcus aureus* Biofilm Matrix by Subinhibitory Concentrations of Clindamycin. *Antimicrob Agents Chemother* 60:5957–5967. <https://doi.org/10.1128/AAC.00463-16>
- Sergei MM (2001) DNA Topology: Fundamentals. In e LS, (Ed.). <https://doi.org/https://doi.org/10.1038/npg.els.0001038>
- Shahabadi N, Hashempour S (2019) DNA binding studies of antibiotic drug cephalixin using spectroscopic and molecular docking techniques. *Nucleosides Nucleotides*

- Nucleic Acids 38(6):428–447. <https://doi.org/10.1080/15257770.2018.1562071>
- Shang W, Rao Y, Zheng Y, Yang Y, Hu Q, Hu Z, Yuan J, Peng H, Xiong K, Tan L, Li S, Zhu J, Li M, Hu X, Mao X, Rao X (2019) β -Lactam Antibiotics Enhance the Pathogenicity of Methicillin-Resistant *Staphylococcus aureus* via SarA-Controlled Lipoprotein-Like Cluster Expression. mBio. Doi: <https://doi.org/10.1128/mBio.00880-19>
- Silver S (2003) Bacterial silver resistance: molecular biology and uses and misuses of silver compounds. FEMS Microbiol Rev 27:341–353. [https://doi.org/10.1016/S0168-6445\(03\)00047-0](https://doi.org/10.1016/S0168-6445(03)00047-0)
- Suh D, Chaires JB (1995) Criteria for the mode of binding of DNA binding agents. Bioorg Med Chem 3:723–728. [https://doi.org/10.1016/0968-0896\(95\)00053-J](https://doi.org/10.1016/0968-0896(95)00053-J)
- Sullivan M, Kia AFA, Long M, Walsh M, Kavanagh K, McClean S, Creaven BS (2014) Isolation and characterisation of silver(I) complexes of substituted coumarin-4-carboxylates which are effective against *Pseudomonas aeruginosa* biofilms. Polyhedron 67:549–559. <https://doi.org/10.1016/j.poly.2013.09.042>
- Wadt WR, Hay PJ (1985) *Ab initio* effective core potentials for molecular calculations. Potentials for main group elements Na to Bi. J Chem Phys 82:284–298. <https://doi.org/10.1063/1.448800>
- Wang S, Shao W, Li H, Liu C, Wang K, Zhang J (2011) Synthesis, Characterization and Cytotoxicity of the Gold(III) Complexes of 4,5-dihydropyrazole-1-carbothioamide Derivatives. Eur J Med Chem 46:1914–1918. <https://doi.org/10.1016/j.ejmech.2011.02.031>
- Waring MJ (1991) Binding of antibiotics to DNA, Ciba Foundation symposium 158:128–42; <https://doi.org/https://doi.org/10.1002/9780470514085.ch9>
- WHO factsheet sepsis, <https://www.who.int/news-room/factsheets/detail/sepsis>. Accessed 1 Nov 2018
- Wu H, Yuan J, Bai Y, Pan G, Wang H, Kong J, Fan X, Liu H (2012) Synthesis, structure, DNA-binding properties and antioxidant activity of silver(I) complexes containing V-shaped bis-benzimidazole ligands. Dalton Trans 41:8829–8838. <https://doi.org/10.1039/c2dt30512g>
- Wu H, Zhang J, Chen C, Zhang H, Peng H, Wang F, Yang Z (2015) Synthesis, crystal structure, and DNA-binding studies of different coordinate binuclear silver(I) complexes with benzimidazole open-chain ether ligands. New J Chem 39:7172–7181. <https://doi.org/10.1039/c5nj01684c>
- Yang L, Liu Y, Wu H, Song Z, Høiby N, Molin S, Givskov M (2012) Combating biofilms. FEMS Immunol Med Microbiol 65:146–157. <https://doi.org/10.1111/j.1574-695X.2011.00858.x>

Publisher's Note Springer Nature remains neutral with regard to jurisdictional claims in published maps and institutional affiliations.